Amino Acid Derivatives of Tetrathiafulvalene and Their N-H center dot center dot center dot O Peptide Bond Dipoles-Templated Solid State Assemblies

Abdelkrim El-Ghayoury, Leokadiya Zorina, Sergey Simonov, Lionel Sanguinet, Patrick Batail

EurJOC European Journal of Organic Chemistry

FULL PAPER

DOI: 10.1002/ejoc.201201330

Amino Acid Derivatives of Tetrathiafulvalene and Their N–H···O Peptide Bond Dipoles-Templated Solid State Assemblies

Abdelkrim El-Ghayoury,*[a] Leokadiya Zorina,[b] Sergey Simonov,[b] Lionel Sanguinet,[a] and Patrick Batail*[a]

Keywords: Amino acids / Solid-state structures / Sulfur heterocycles / Hydrogen bonds / Peptides

We report on a series of amino acid derivatives of tetrathiafulvalene as well as on the structure-directing abilities of their peptide residues in the crystalline solid state to stabilize patterns of interactions such as β strands and sheet motifs. Characteristic hydrogen-bonding motifs are indeed identified within ethylenedithiotetrathiafulvalene (EDT-TTF) and dimethyltetrathiafulvalene (Me_2-TTF) based compounds **1**–**5**. Esters **1**–**3** contain hydrogen-bond acceptors, namely carbonyl groups, as well as one strong (NH) and one weak (C_{sp^2}–H) hydrogen-bond donor. In addition to the hydrogen-bonded sets of ester derivatives, acids **4** and **5** present the carboxylic acid moiety, which acts as both a hydrogen-bond donor and acceptor. EDT-TTF-CO-GlyOH has been previously used to afford a new type of hydrogen-bonded acid/zwitterion (1:1) hybrid admixture of redox peptidics.

Introduction

The chemistry of organic π donors based on tetrathiafulvalene (TTF) and its derivatives has been the subject of numerous studies because of their use as precursors to molecular conductors and superconductors.[1] It is well established that intermolecular interactions such as a p_π–p_π orbital overlap within the stacks or slabs and hydrogen and halogen bonds play a prominent role in governing the electronic properties of these crystalline materials. Thus, efforts have been devoted to direct the intermolecular interactions in both the neutral closed-shell molecules as well as in the corresponding charge-transfer complexes and radical cation salts.[2] Tetrathiafulvalene derivatives bearing substituents that can participate in hydrogen-bonding interactions have been actively investigated. Examples of these molecules bearing functionalities with strong hydrogen-bonding capabilities are (i) the alcohols Me_3TTF(CHMeOH),[3] TTF$(CH_2OH)_4$,[4] and EDT-TTF-CH_2OH,[5] (ii) thioamides[6] and mono-[7] and diamides,[8] (iii) uracil-derivatized TTFs[9] and adenine-derivatized TTF,[10] and (iv) the anilinium phosphonate $PhNH_3^+Me_3$TTF-PO_3H^- along with its one-electron oxidation product and the zwitterion $[Me_3TTF\text{-}PO_3H^-]^+$.[11]

Recently, the templating effect of N–H···O peptide bond dipoles has been shown to direct the formation of stacks of amino acid derivatives of perylenediimide into solid state assemblies.[12] However, few amino acid-appended tetrathiafulvalene systems have been investigated in this context. These include TTF with a polypeptide backbone[13] and TTF bearing a methyl ester amino acid.[14] Electroactive supramolecular fibers have been described as well.[15] Recently, we have shown that the attachment of an amino acid to an EDT-TTF (ethylenedithiotetrathiafulvalene) unit leads to neutral zwitterionic molecular solids in which the stoichiometry and structure are directed by hydrogen-bonding interactions of the ionizable amino acid residues.[16]

Herein, we report on the chemistry and crystal structures of a series of amino acid-appended TTFs and evaluate the structure-directing ability of the peptide residues to form patterns of supramolecular interactions such as β strands and sheet motifs.[17] Of particular note, the hydrogen-bonded, acid/zwitterion (1:1) hybrid admixture of redox peptidics is disclosed therein.

Results and Discussion

The synthetic protocol for the EDT-TTF ester derivative was adapted from a previously described procedure for the synthesis of EDT-TTF amides.[18] The EDT-TTF core was chosen because of its well-known ability to direct the formation of layered structures, whereas a Me_2-TTF (dimethyltetrathiafulvalene) motif favors the formation of radical

[a] LUNAM Université, Université d'Angers, CNRS UMR 6200, Laboratoire MOLTECH-Anjou,
2 Bd. Lavoisier, 49045 Angers Cedex, France
Fax: +33-2-41735405
E-mail: abdelkrim.elghayoury@univ-angers.fr
patrick.batail@univ-angers.fr
Homepage: http://moltech-anjou.univ-angers.fr/
[b] Institute of Solid State Physics RAS,
142432 Chernogolovka MD, Russia

Supporting information for this article is available on the WWW under http://dx.doi.org/10.1002/ejoc.201201330.

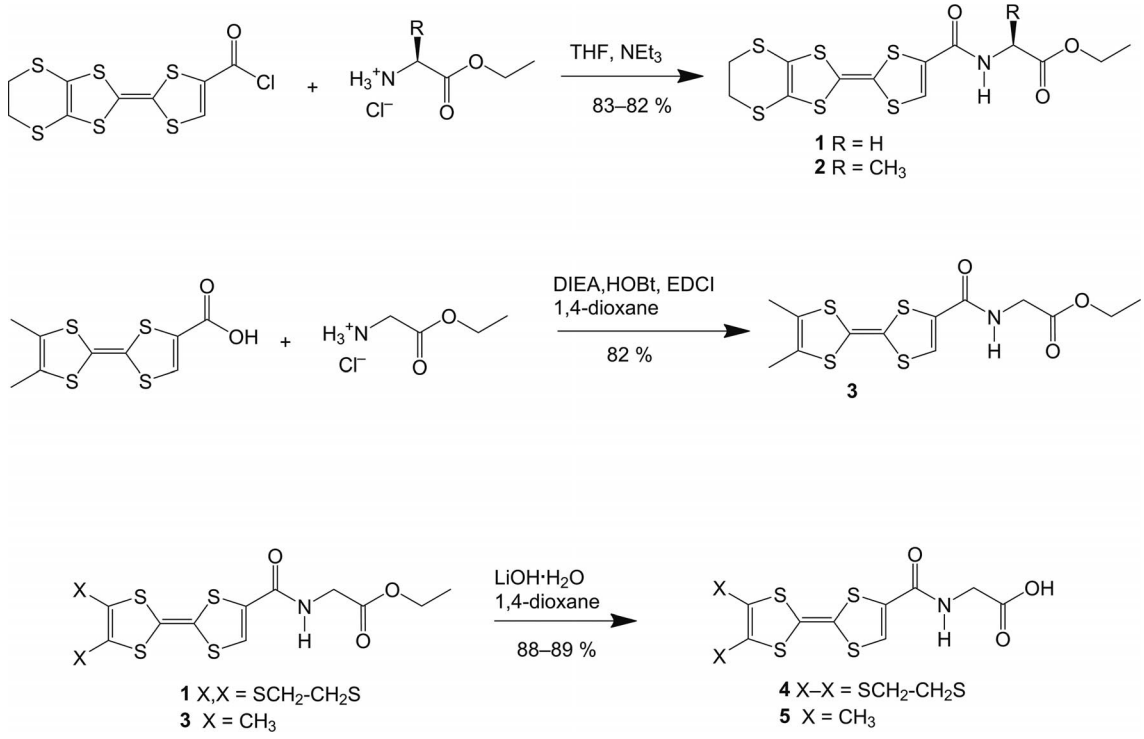

Scheme 1. Synthetic scheme for compounds **1**–**5**.

cation stacks.[19] As shown in Scheme 1, amido ester derivatives **1** and **2** were prepared by the reaction of EDT-TTF acid chloride, whose synthesis has been previously described,[20] and either commercially available glycine ethyl ester hydrochloride or alanine ethyl ester hydrochloride in the presence of triethylamine. Amido ester **3** was prepared by essentially following the procedure described by Moroder,[21] which involved coupling Me_2-TTF carboxylic acid[22] and glycine ethyl ester hydrochloride under peptidic coupling conditions. The hydrolysis to the corresponding amido acids **4** and **5** was performed by using LiOH in a mixture of water and dioxane.

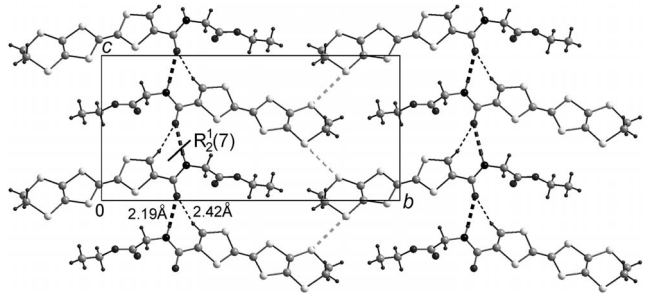

Figure 1. Tweezer-like pattern of hydrogen-bonding interactions and S···S contacts in the *bc* layer of **1**. Similar checkerboard layers with tweezer-like hydrogen bonds have also been found in ester compounds **2** and **3** as well as in TTF-CO-GlyMe.[14]

Molecular Geometry for 1–5

All of the compounds were obtained as single crystals, and a complete analysis of their structures was carried out on the basis of X-ray diffraction data (Table 4). Table 2 describes the molecular geometry of compounds **1**–**5**. The inner C=C double bond lengths (*d*) within the TTF cores correspond to a neutral molecular state. EDT-TTF and Me_2-TTF fragments in **1**–**5** exhibit various degrees of bending about the S-S vectors (α_1 and α_2 values), as expected for neutral TTF-based molecules. The functional groups have a pronounced twist with respect to the TTF mean plane, and the planar acid moiety is almost perpendicular to the TTF core (for instance, see Figure 1). The corresponding torsion angles β_1 (between TTF and the amide group), β_2 (between the amide and acid moieties), and β_3 (between the acid and ester parts in **1**–**3**) are also listed in Table 1.

Table 1. Molecular geometry for **1**–**5**. Central C=C double bond lengths (*d*) in TTF fragment and dihedral (α_1, α_2) and torsion (β_1, β_2, β_3) angles.

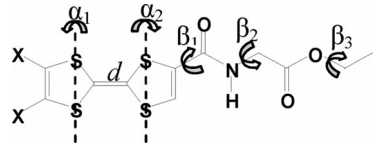

	d [Å]	α_1 [°]	α_2 [°]	β_1 [°]	β_2 [°]	β_3 [°]
1	1.342(3)	0.93(4)	4.82(6)	19.4(3)	98.6(3)	10.6(2)
2/I	1.339(5)	5.85(2)	6.00(3)	7.1(6)	78.8(4)	10.5(4)
2/II	1.333(5)	9.31(2)	1.21(3)	6.1(6)	85.7(5)	7.8(4)
3/I	1.341(3)	3.17(4)	23.56(3)	–17.4(3)	91.5(2)	–14.1(2)
3/II	1.339(3)	1.88(5)	1.07(5)	–5.7(3)	98.8(2)	–2.5(2)
4	1.334(4)	5.43(5)	4.61(8)	–17.4(5)	102.9(4)	–
5/I	1.342(3)	1.02(7)	10.69(6)	15.5(4)	–106.8(3)	–
5/II	1.339(3)	9.04(6)	29.30(5)	22.4(4)	106.2(3)	–

N–H···O Peptide Bond Dipoles and their Complementary Hydrogen-Bonding Schemes in 1–5

The primary noncovalent intermolecular interaction directing the self-assembly in the solid state of esters **1**–**3** originates from the amide N–H, the strongest hydrogen-bond donor. This interaction is complemented by a weaker hydrogen-bond donor (C_{sp^2}–H) and the carbonyl group, a hydrogen-bond acceptor. In addition, the carboxylic acid group in **4** and **5** acts as both a hydrogen-bond donor and acceptor (Scheme 2). Note that the acid residues are ionizable and, as such, can be used as templating bases for the preparation of neutral zwitterionic solids[16] or engaged as charge-compensating functional anions in radical cation salts.[23]

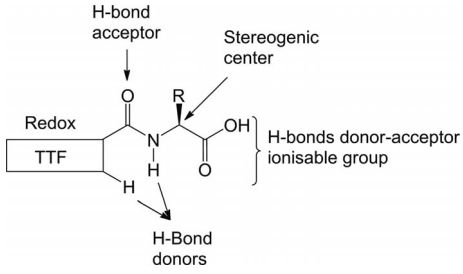

Scheme 2. Multifunctional TTF-appended amino acid derivatives.

Three types of hydrogen-bonding patterns are identified in **1**–**5** (Scheme 3) and noted according to Etter's nomenclature as $R_d^a(n)$.[24] The cyclic motifs, $R_2^1(7)$, that are found with many TTF-based amides[2] direct the structural organization of esters **1**–**3**. A typical carboxylic acid dimer, $R_2^2(8)$, is formed with acid **4**, and a rare hydrogen-bonding pattern, $R_2^2(14)$, is found with acid **5**.

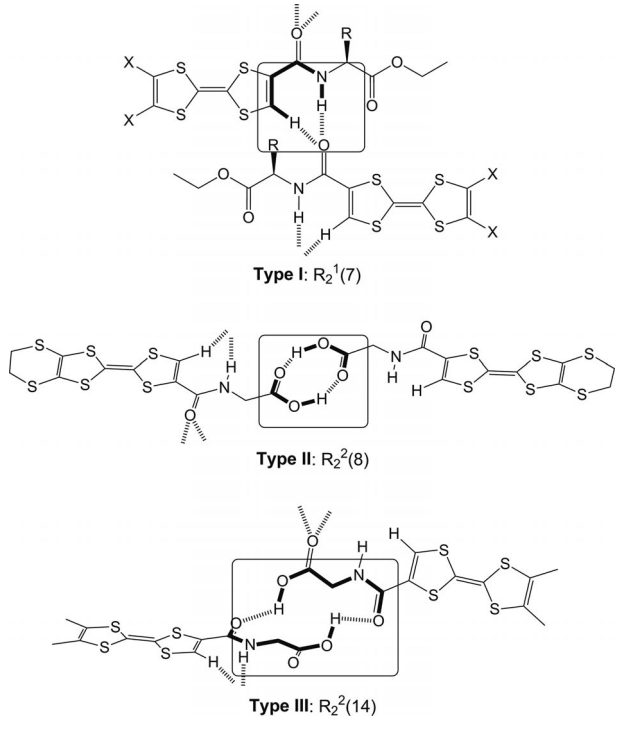

Scheme 3. The three types of hydrogen-bonding patterns characteristic of the series.

Layered Structures of Esters 1–3

The structures of the amido ester derivatives of EDT-TTF (i.e., **1** and **2**) and Me_2-TTF (i.e., **3**) have topologically similar layers in the *bc* plane, which stand out as a common structural feature, and the ester molecules are connected into infinite chains through hydrogen bonds. Within a layer (Figure 1), all of the functional groups are interleaved with EDT-TTF fragments along both the *b* and *c* directions forming a checkerboard pattern. Large collections of parallel N–H···O peptide bond dipoles are the primary structure-directing intermolecular interactions in **1**–**3** (see Table 2 for geometry of hydrogen bonds). In combination with the weaker C_{sp^2}–H···O contacts, they produce a typical tweezer-like $R_2^1(7)$ cyclic motif.

Table 2. Geometry of intermolecular D–H···O hydrogen bond contacts (<2.7 Å) in **1**–**5**.

	D–H···A	H···A [Å]	D···A [Å]	D–H···A [°]
1	$N–H_{amide}···O_{amide}$	2.19	3.038(2)	169.3
	$C_{sp^2}–H_{TTF}···O_{amide}$	2.42	3.193(3)	140.3
2/I	$N–H_{amide}···O_{amide}$	2.23	3.023(5)	153.3
	$C_{sp^2}–H_{TTF}···O_{amide}$	2.55	3.453(5)	165.0
	$C_{sp^3}–H_{EDT\text{-}TTF}···O_{ester}$	2.34	3.187(9)	145.4
	$C_{sp^3}–H_{EDT\text{-}TTF}···O_{ester}$	2.40	3.079(17)	126.7
2/II	$N–H_{amide}···O_{amide}$	2.33	3.059(5)	142.9
	$C_{sp^2}–H_{TTF}···O_{amide}$	2.63	3.488(5)	153.3
	$C_{sp^3}–H_{EDT\text{-}TTF}···O_{ester}$	2.51	3.172(6)	125.2
3/I	$N–H_{amide}···O_{amide}$	2.13	2.963(2)	163.6
	$C_{sp^2}–H_{TTF}···O_{amide}$	2.31	3.101(2)	142.7
	$C_{sp^3}–H_{Me_2\text{-}TTF}···O_{ester}$	2.66	3.600(3)	166.1
3/II	$N–H_{amide}···O_{amide}$	2.23	3.079(2)	169.5
	$C_{sp^2}–H_{TTF}···O_{amide}$	2.30	3.228(2)	171.7
	$C_{sp^3}–H_{Me_2\text{-}TTF}···O_{ester}$	2.71	3.665(3)	172.9
4	$O–H_{acid}···O_{acid}$	1.79(5)	2.712(4)	163(4)
	$N–H_{amide}···O_{amide}$	2.09(2)	2.911(3)	168(3)
	$C_{sp^2}–H_{TTF}···O_{amide}$	2.38(3)	3.178(4)	150(3)
5/I	$O–H_{acid}···O_{amide}$	1.88	2.683(3)	166.9
	$N–H_{amide}···O_{amide}$	2.13	2.861(3)	142.5
	$C_{sp^2}–H_{TTF}···O_{amide}$	2.68	3.364(3)	131.5
	$C_{sp^2}–H_{TTF}···O_{acid}$	2.52	3.284(3)	139.4
	$C_{sp^3}–H_{Me_2\text{-}TTF}···O_{acid}$	2.50	3.431(3)	162.0
5/II	$O–H_{acid}···O_{amide}$	1.92	2.727(2)	166.5
	$N–H_{amide}···O_{acid}$	2.09	2.926(3)	165.6
	$C_{sp^2}–H_{TTF}···O_{acid}$	2.45	3.286(3)	150.3
	$C_{sp^3}–H_{acid}···O_{acid}$	2.55	3.337(3)	137.8

The three ester structures of **1**–**3**, which have similar layers and the $R_2^1(7)$ type of hydrogen bonding (Figure 1), differ in their symmetry and some structural details. The *bc* layer is constructed from either one independent molecule in the monoclinic $P2_1/c$ structure for **1** or two independent molecules in both the noncentrosymmetric monoclinic $P2_1$ structure for chiral molecule **2** (*S* enantiomer) and the triclinic $P\bar{1}$ structure for **3**, and all of the molecules are in general positions. In **1** and **3**, the layers are corrugated [dihedral angles between mean planes of neighboring TTFs

within the *bc* layer are 21.61(3)° in **1** and 45.94(1)° in **3**], whereas all of the TTF fragments in a layer of **2** are nearly parallel. Molecules of **1** form interlayer centrosymmetric dimers with head-to-tail overlap of the EDT-TTF cores. In the structures of **2** and **3**, infinite molecular stacks along the *a* axis are formed. A side view of two independent stacks in the structure of **3** (Figure 2, a and b) shows a large difference in the geometry of the two molecules, which demonstrates a high degree of molecular freedom in adapting to the environment in the crystal. For example, molecule II is much more planar than I (Table 2), and the amido ester groups, located between the stacks, extend in very different directions within I and II.

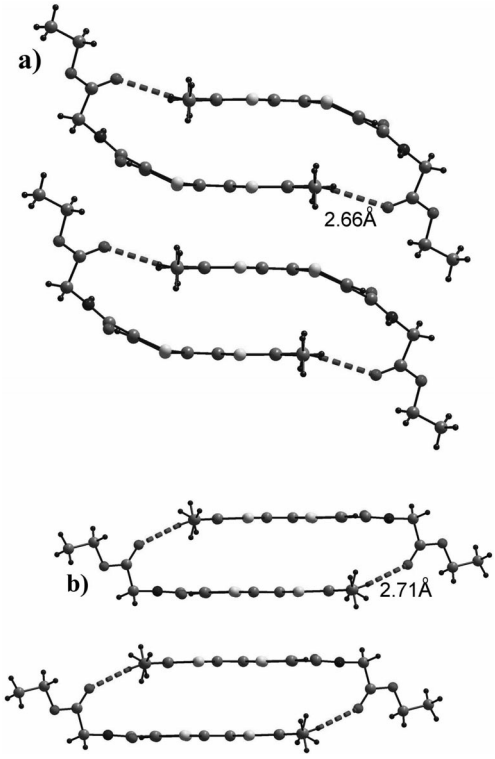

Figure 2. Side view of the molecular stack formed along the *a* direction in the structure of ester **3**: (a) stack I and (b) stack II. Hydrogen-bonding contacts between methyl groups of the TTF core and oxygen atom of the carboxy group are shown by dashed lines. The geometry of the hydrogen bond is described in Table 3.

In the structure of **1**, only the amide group acts as an active hydrogen-bond donor and acceptor, whereas all of the other hydrogen-bonding contacts have H···O distances not less than 2.85 Å. In **2** and **3**, additional intrastack hydrogen-bonding contacts (C_{sp^3}–H···O_{ester}) between the outer ethylene groups of EDT-TTF or the methyl groups of Me_2-TTF and the carbonyl oxygen atoms of the ester group are observed (Figure 2) and characterized in Table 2. It should be noted that the S···S intermolecular interactions, which are typical for TTF-based molecular conductors, are not found in the structures of the esters **1**–**3**, with the exception of one S···S contact of 3.5259(9) Å in the *bc* layer of **1** (Figure 1).

Synergy between Two Hydrogen-Bonding Patterns in the Crystal Structure of Acid 4

Two types of hydrogen-bonding patterns are working in unison in **4** (Figure 3), and the structure of **4** differs in this respect from the structure of the corresponding ester **1** (Figure 1). A tweezer-like $R_2^1(7)$ motif, which describes the structures of esters **1**–**3**, is found between the molecules along the *c* direction. However, the strongest hydrogen bonds of the type O–H···O (Table 2) are formed between the acid functions, which give rise to the classic carboxylic acid eight-membered $R_2^2(8)$ motif.

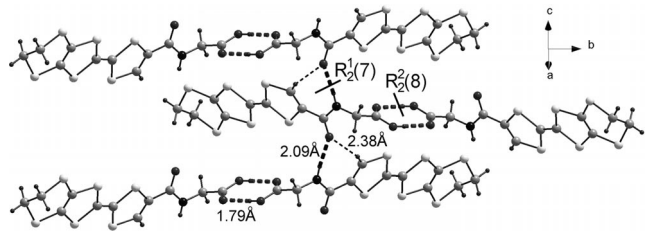

Figure 3. Two hydrogen-bonding motifs in **4**.

It is of interest to note that the crystal structures of **1** and **4** have the same monoclinic $P2_1/c$ space group, rather close unit cell parameters (taking into account the difference in molecular composition), and similar principles of structural organization. The main difference between the crystal structures is caused by the presence of the COOH function in **4**, a strong hydrogen-bond donor and acceptor, instead of less active ester group in **1**. This results in additional strong hydrogen bonds in the structure of **4** (compare Figures 1 and 3). In contrast to the dimeric structure of the corresponding ester **1**, the combination of the two hydrogen-bonding motifs in **4** efficiently templates infinite stacks along the *a* axis, where the acid molecules are related by inversion. The molecules from adjacent stacks along the *bc* diagonals are not parallel, and the dihedral angle between the mean planes of their TTF cores amounts to 64.04(2)°. In spite of being at rather close interplanar distances, 3.53(1) and 3.58(1) Å, the molecules inside the stack do not form any shortened S···S contacts, and the structure of **4** is controlled only by interstack hydrogen bonding.

A Rather Unique Organization of Hydrogen Bonds in the Structure of Acid 5

The crystal structure of **5** (monoclinic $P2_1/n$) differs considerably from the structures of the other four molecules. The Me_2-TTF fragments of the two independent molecules (i.e., I and II), which are located in general positions, are combined into the layers parallel to the *ab* plane and interleaved along the *c* direction with the amino acid fragments (Figure 4). The topology of the layers resembles that of the well-known κ-type packing arrangement in organic conductors (Figure 5). The layer is formed by two independent, centrosymmetric and essentially orthogonal [dihedral angle, 86.47(2)°] dimeric units I and II with intradimer interplanar separations of 3.63(1) and 3.96(2) Å, respectively. The large

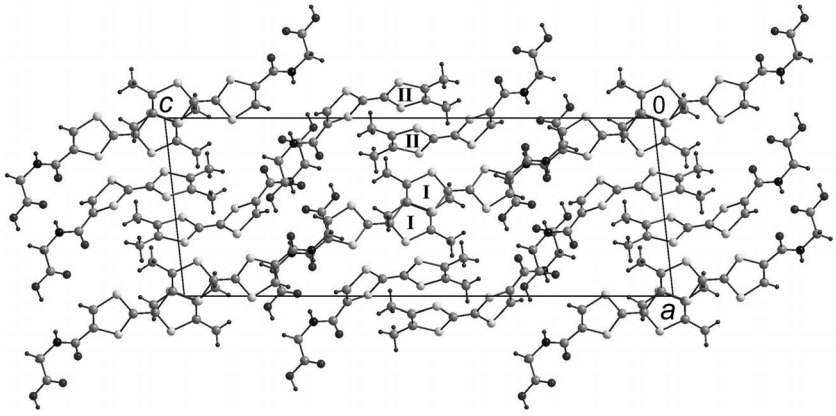

Figure 4. Projection of the structure of **5** along the *b* direction. As exemplified further in Figure 5, layers of Me_2-TTF fragments assemble into a κ-type topology parallel to the *ab* plane.

relative longitudinal displacement of the molecules inside of the dimers is equal to approximately 6 Å in I and 4 Å in II (Figure 4). This leads to the absence of shortened intradimer contacts, that is, all of the S···S distances are over 4 Å. In addition, the functional groups are directed outside or inside the dimers in I and II, respectively.

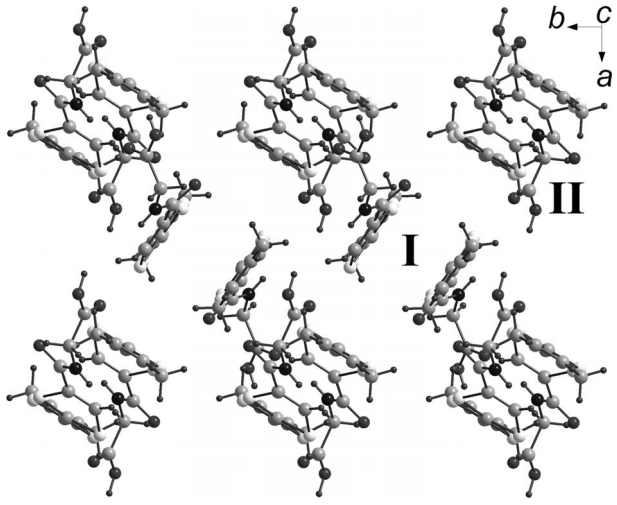

Figure 5. κ-Type layer of molecules of **5** viewed along the long Me_2-TTF axis. The layer consists of two nonequivalent orthogonal molecular dimers I and II.

A pair of molecules I and II from adjacent layers in **5** interact primarily by the N–H···O peptide bonds across the layers along the *c* direction (Figure 6). Remarkably, the two acid groups are not interlocked with each other into a $R_2^2(8)$ motif like in the structure of **4** and many other neutral and oxidized carboxylic acid TTF-derivatives.[2] Each of the two OH groups prefers to interact instead with an amide oxygen atom of a neighboring molecule by a strong O_{acid}–H···O_{amide} bond (Table 2), which results in the formation of the rare $R_2^2(14)$ motif that is represented by the large fourteen-membered grey cycles in Figure 6. This motif has been previously described in only two structures.[25] Tweezer-like hydrogen bonds are formed by both molecules, but include diverse hydrogen-bond acceptor atoms. A pair of NH and $C_{sp^2}H$ functions in I hold the amide oxygen of another molecule I, whereas the same pair of hydrogen-bond donor groups in II is connected to the acid oxygen atom of I, which protrudes out of the $R_2^2(14)$ cycle (Figure 6). The carbonyl oxygen atom of molecule II acts as a hydrogen-bond acceptor for the two C_{sp^2}–H···O and C_{sp^3}–H···O contacts. Table 2 describes the geometry for all of these bonds.

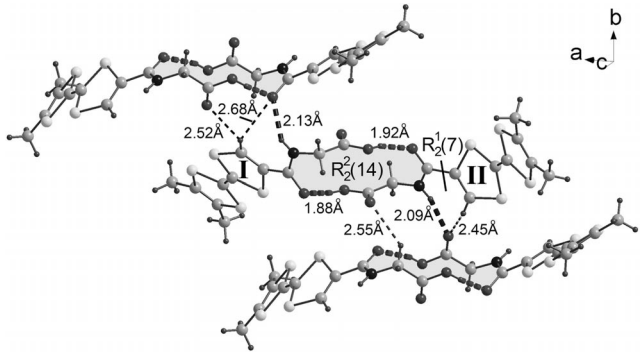

Figure 6. Hydrogen-bonding pattern in **5**. Molecules I and II from adjacent layers are linked by pairs of strong O–H···O hydrogen bonds, which form the $R_2^2(14)$ cyclic motifs shown in grey.

Comparison of Crystal Structures 1–5

Some general conclusions can be drawn by analyzing and comparing the crystal structures of this series of TTF-amino acid derivatives. First, the structures of **1**–**5** are primarily governed by hydrogen bonding, whereas the S···S interactions, which dominate in nonfunctionalized TTF-based crystals, are found to be only in a subordinate position in **1** (Figure 1) or a negligible one in **2**–**5**. This is in spite of the fact that π···π stacking exists in the dimeric units (in **1**) or infinite stacks (in **2**–**5**) in all the structures. Three types of hydrogen-bonding motifs based on N–H···O, O–H···O, and C_{sp^2}–H···O bonds were found (Scheme 3). The O–H···O bonds, established by the participation of the OH group of acid moiety as the hydrogen-bond donor and acid or amide oxygen as the hydrogen-bond acceptor, are the strongest ones in comparison to the other hydrogen bonds

(Table 2). However, the COOH function, the most active hydrogen-bond competitor in the TTF-based amido acids **4** and **5**, is deactivated in ethyl esters **1**–**3**. At the same time, the classical N–H···O peptide bond dipole,[12] which connects the neighboring amide CONH fragments, stands out as the primary structure-directing element. This is a consequence of the strong hydrogen-bond donor and acceptor roles of the amide function in all of the known amido acid and amido ester TTF-derivatives, independent of their composition, including the structures of **1**–**5** and TTF-CO-GlyMe.[14]

Oxidation Potentials

Cyclic voltammetry experiments were performed to evaluate the oxidation potentials of the new donor molecules and the influence of the ester and acid functionality on the redox properties of the EDT-TTF or Me_2-TTF core. The corresponding half-wave potentials for all of the compounds along with those of EDT-TTF for comparison are listed in Table 3. All of the EDT-TTF derivatives **1**, **2**, and **4** oxidize reversibly at about the same potential without any substantial difference between the ester and acid moieties. Compared with that of EDT-TTF, the first oxidation potential is anodically shifted by 50–80 mV, as in the case of EDT-TTF amides. The Me_2-TTF derivatives **3** and **5** do oxidize reversibly at the same potential. Compared with the parent Me_2-TTF, the first oxidation potential is also anodically shifted by 88 mV. These electrochemical results confirm the electron-withdrawing effect of an amido group that is directly linked to the TTF moieties and the almost no direct effect of the terminal ester or acid group. These results indicate that these molecules are capable, upon electrochemical oxidation, to form stable radical cation salts. The acid derivatives, because of the ionizable acid group, are able in combination with templating bases with various pH activities to form monocomponent systems (neutral zwitterionic) or two-component radical cation salts. In fact, in the electrochemical oxidation of acid **4** using tetrabutylammonium fumarate as an electrolyte and especially as a base, we successfully obtained a neutral zwitterionic solid.[16] The use of other bases with different pH activities such as sulfates or phosphates are under investigation to prepare two-component radical cation salts.

Table 3. Oxidation potentials (V vs. SCE) for **1**–**5** and two reference compounds.

Compound	$E_{1/2}{}^1$	$E_{1/2}{}^2$
EDT-TTF	0.42	0.610
Me_2-TTF	0.30	0.55
1	0.50	0.62
2	0.48	0.66
3	0.39	0.65
4	0.50	0.69
5	0.39	0.65

Conclusions

By appending the tetrathiafulvalene core to an amino acid, we expected to take advantage, as we have already shown for acid **4**,[16] of the versatile structure-directing ability of the amino acid residues, which are prone to self-organize, by stabilizing robust peptidic bonding patterns such as β-strand motifs. The presence of both the amido and carboxylic acid groups is of great importance to explore the outcome of competing hydrogen-bonding interactions in the crystal structures of the corresponding neutral solids. In combination with an appropriate base, the acid derivatives are of great importance for the preparation of neutral zwitterionic solids and two-component radical cation salts that have rich structural and physical properties.

Experimental Section

Ethyl Ethylenedithiotetrathiafulvaleneamidoglycinate (EDT-TTF-CO-GlyOEt, 1): In a three-necked flask under nitrogen, ethyl glycinate hydrochloride (0.500 g, 1.43 mmol) was suspended in freshly distilled tetrahydrofuran (20 mL), and to this mixture was added triethylamine (1 mL). A solution of ethylenedithiotetrathiafulvalene acid chloride (0.500 g, 1.40 mmol) in tetrahydrofuran (30 mL) was added dropwise. The mixture was stirred overnight, and the tetrahydrofuran (THF) was removed by distillation under vacuum. The resulting mixture was extracted from water with dichloromethane (3 × 75 mL). The combined organic phases were dried with sodium sulfate, and the solvent was evaporated under vacuum to afford an orange-red solid. Recrystallization from a hot acetonitrile solution yielded orange-red single crystals of EDT-TTF-CO-GlyOEt (0.490 g, 83%) that were suitable for X-ray crystal structure analysis. UV/Vis (CH_3CN): λ_{max} (ε, $dm^3\,mol^{-1}\,cm^{-1}$) = 306 (17900), 327 (13800), 399 (sh) nm. IR (selected bands): $\tilde{\nu}$ = 3318.1, 2973.4, 1741.9, 1626.6, 1550.2, 1398.7, 1304.4, 1199.6cm^{-1}. ^1H NMR (500.13 MHz, [D_6]DMSO, 25 °C): δ = 9.02 (t, J = 5.84 Hz, 1 H), 7.61 (s, 1 H), 4.10 (q, J = 7.11 Hz, J = 4.28 Hz, 2 H), 3.89 (d, J = 5.83 Hz, 2 H), 3.39 (s, 4 H), 1.18 (t, J = 7.09 Hz, 3 H) ppm. $^{13}C\{^1H\}$ NMR (125 MHz, [D_6]DMSO, 25 °C): δ = 169.4 (O-C=O), 159.2 (N-C=O), 132.3 (=C-CO), 126.0 (=CH), 116.1–104.0 (C=C), 60.7 (O-CH_2), 41.1 (N-CH_2), 29.5 (CH_2-CH_2), 14.1 (CH_3) ppm. $C_{13}H_{13}NO_3S_6$ (423.61): calcd. C 36.86, H 3.09, N 3.31; found C 36.92, H 2.99, N 3.40. MS (MALDI-TOF): calcd. for $[M]^+$ 422.92; found 422.76.

Ethyl Ethylenedithiotetrathiafulvaleneamidoalaninate (EDT-TTF-CO-AlaOEt, 2): In a three-necked flask under nitrogen, ethyl alaninate hydrochloride (0.11 g, 0.72 mmol) was suspended in freshly distilled tetrahydrofuran (10 mL), and to this mixture was added triethylamine (1 mL). A solution of ethylenedithiotetrathiafulvalene acid chloride (0.25 g, 0.70 mmol) in tetrahydrofuran (20 mL) was added dropwise. The mixture was stirred overnight, and THF was removed by distillation under vacuum. The resulting mixture was extracted from water with dichloromethane (3 × 75 mL). The combined organic phases were dried with sodium sulfate, and the solvent was evaporated under vacuum to afford an orange-red solid. Recrystallization from a hot acetonitrile solution yielded orange-red single crystals of **2** (0.25 g, 82%) that were suitable for X-ray crystal structure analysis. UV/Vis (CH_3CN): λ_{max} (ε, $dm^3\,mol^{-1}\,cm^{-1}$) = 306 (15800), 327 (13100), 390 (sh) nm. IR (se-

lected bands): $\tilde{\nu}$ = 3286.0, 2978.3, 1741.8, 1624.6, 1545.0, 1368.2, 1269.8, 1198.8 cm^{-1}. ^1H NMR (500.13 MHz, [D$_6$]DMSO, 25 °C): δ = 8.93 (d, J = 6.86 Hz, 1 H), 7.68 (s, 1 H), 4.28 (m, 1 H), 4.08 (m, 2 H), 3.39 (s, 4 H), 1.32 (d, J = 7.31 Hz, 3 H), 1.17 (t, J = 7.11 Hz, 3 H) ppm. $^{13}C\{^1H\}$ NMR (125 MHz, [D$_6$]DMSO, 25 °C): δ = 172.4 (O-C=O), 158.9 (N-C=O), 133.0 (=C-CO), 116.3–104.0 (C=C), 60.9 (O-CH_2), 48.6 (N-CH), 45.7 (CH_3), 29.7 (CH_2-CH_2), 14.3 (CH_3) ppm. $C_{14}H_{15}NO_3S_6$ (437.64): calcd. C 38.42, H 3.45, N 3.20; found C 38.50, H 3.82, N 3.15. MS (MALDI-TOF): calcd. for $[M]^+$ 436.9; found 437.0.

Ethyl Dimethyltetrathiafulvaleneamidoglycinate (Me$_2$-TTF-CO-GlyOEt, 3): To a solution of Me$_2$-TTF-CO_2H (0.60 g, 2.17 mmol) in 1,4-dioxane (30 mL) were successively added *N*,*N*-diisopropylethylamine (DIEA, 0.94 g, 7.2 mmol), 1-hydroxybenzotriazole (HOBt, 0.33 g, 2.4 mmol), 1-ethyl-3-(3-dimethylaminopropyl)-carbodiimide (EDCI, 0.46 g, 2.4 mmol), and ethyl glycinate hydrochloride (0.304 g, 2.18 mmol). After stirring for 15 h under nitrogen, the solvent was removed, and the residue was extracted from water with ethyl acetate. The combined organic layers were washed with $NaHCO_3$ (5% solution), $KHSO_4$ (5% solution), and water and then dried with $MgSO_4$. The solvent was evaporated under vacuum to dryness. Recrystallization from a hot acetonitrile solution yielded dark red, single crystals of Me$_2$-TTF-CO-GlyOEt (0.65 g, 82%) that were suitable for X-ray crystal structure analysis. UV/Vis (CH_3CN): λ_{max} (ε, $dm^3 mol^{-1} cm^{-1}$) = 312 (16150), 411 (sh) nm. IR (selected bands): $\tilde{\nu}$ = 3304.7, 3034.0, 1745.0, 1619.2, 1560.3, 1371.9, 1307.6, 1199.0 cm^{-1}. ^1H NMR (500.13 MHz, [D$_6$]DMSO, 25 °C): δ = 8.91 (t, J = 5.86 Hz, 1 H), 7.53 (s, 1 H), 4.09 (q, J = 7.11 Hz, J = 4.28 Hz, 2 H), 3.88 (d, J = 5.87 Hz, 2 H), 1.94 (s, 6 H), 1.18 (t, J = 7.12 Hz, 3 H) ppm. $^{13}C\{^1H\}$ NMR (125 MHz, [D$_6$]DMSO, 25 °C): δ = 169.5 (O-C=O), 159.3 (N-C=O), 132.8 (=C-CO), 126.3 (=CH), 123.5–106.6 (C=C), 60.6 (O-CH_2), 41.1 (N-CH_2), 14.1 (CH_3), 13.1 (CH_3) ppm. $C_{13}H_{15}NO_3S_4$ (361.51): calcd. C 43.19, H 4.18, N 3.87; found C 42.88, H 4.03, N 4.11. MS (MALDI-TOF): calcd. for $[M]^+$ 361.5; found 361.1.

Ethylenedithiotetrathiafulvaleneamidoglycine (EDT-TTF-CO-GlyOH, 4): To a solution of EDT-TTF-CO-GlyOEt (0.17 g, 0.40 mmol) in 1,4-dioxane (20 mL) was added an aqueous solution of lithium hydroxide (0.02 g, 0.48 mmol) in water (3 mL). After stirring for 15 h at room temperature, hydrochloric acid (5 M solution, 5 mL) was added, and the stirring was continued for 5 min. The crude product was then extracted with ethyl acetate (3 × 50 mL). The combined organic layers were dried with sodium sulfate, and the solvent was evaporated, but the process was stopped before the appearance of any solid. The concentrated mixture was allowed to evaporate slowly to yield tiny orange, single crystals of **4** (0.14 g, 88%) that were suitable for X-ray crystal structure analysis. UV/Vis (CH_3CN): λ_{max} (ε, $dm^3 mol^{-1} cm^{-1}$) = 306 (11900), 327 (9300), 399 (sh) nm. IR (selected bands): $\tilde{\nu}$ = 3286.8, 3033.6, 1719.8, 1617.8, 1545.0, 1396.0, 1309.2, 1222.2 cm^{-1}. ^1H NMR (500.13 MHz, [D$_6$]DMSO, 25 °C): δ = 12.70 (s, 1 H), 8.91 (t, J = 5.93 Hz, 1 H), 7.60 (s, 1 H), 3.81 (d, J = 5.92 Hz, 2 H), 3.39 (s, 4 H) ppm. $^{13}C\{^1H\}$ NMR (125 MHz, [D$_6$]DMSO, 25 °C): δ = 170.9 (O-C=O), 159.1 (N-C=O), 132.9 (=C-CO), 125.7 (=CH), 116.1–103.8 (C=C), 66.4 (N-CH_2), 29.5 (CH_2-CH_2) ppm. $C_{11}H_9NO_3S_6$ (395.56): calcd. C 33.40, H 2.29, N 3.54; found C 33.71, H 2.29, N 3.28. MS (MALDI-TOF): calcd. for $[M]^+$ 395.6; found 394.9.

Dimethyltetrathiafulvaleneamidoglycine (Me$_2$-TTF-CO-GlyOH, 5): To a solution of Me$_2$-TTF-CO-GlyOEt (0.100 g, 0.28 mmol) in 1,4-dioxane (10 mL) was added an aqueous solution of lithium hydroxide (0.015 g, 0.38 mmol) in water (3 mL). After stirring for 15 h at room temperature, hydrochloric acid (5 M solution, 5 mL) was added, and the stirring was continued for 5 min. The crude product was then extracted with ethyl acetate (3 × 30 mL). The combined organic layers were dried with sodium sulfate, and the solvent was evaporated, but the process was stopped before the appearance of any precipitate. The homogeneous concentrated solution was allowed to evaporate slowly to yield tiny dark orange single crystals of **5** (0.083 g, 89%) that were suitable for X-ray crystal structure analysis. UV/Vis (CH_3CN): λ_{max} (ε, $dm^3 mol^{-1} cm^{-1}$) = 312 (9770), 417 (sh) nm. IR (selected bands): $\tilde{\nu}$ = 3339.3, 3251.0, 1746.8, 1717.1, 1561.2, 1307.7, 1206.6, 1183.4 cm^{-1}. ^1H NMR (500.13 MHz, [D$_6$]DMSO, 25 °C): δ = 12.70 (s, 1 H), 8.91 (t, J = 5.93 Hz, 1 H), 7.60 (s, 1 H), 3.81 (d, J = 5.92 Hz, 2 H), 3.39 (s, 4 H) ppm. $^{13}C\{^1H\}$ NMR (125 MHz, [D$_6$]DMSO, 25 °C): δ = 171.3 (O-C=O), 159.7 (N-C=O), 133.5 (=C-CO), 126.3 (=CH), 123.5–106.6 (C=C), 41.5 (N-CH_2), 13.9 (CH_3) ppm. $C_{11}H_{11}NO_3S_4$ (333.45): calcd. C 39.96, H 3.32, N 4.20; found C 39.56, H 3.28, N 4.02. MS (MALDI-TOF): calcd. for $[M]^+$ 395.6; found 394.9.

X-ray Crystallographic Studies: Experimental X-ray diffraction data for single crystals of EDT-TTF-CO-GlyOEt (**1**), EDT-TTF-CO-AlaOEt (**2**), Me$_2$-TTF-CO-GlyOEt (**3**), EDT-TTF-CO-GlyOH (**4**), and Me$_2$-TTF-CO-GlyOH (**5**) were collected at room temperature using a Bruker Nonius KappaCCD diffractometer with Mo-K_α radiation (λ = 0.71073 Å, graphite monochromator). The combined ϕ- and ω-scan method was used for the data collection. Empirical absorption correction of experimental intensities was applied for all data using the SADABS program.[26] The structures were solved by a direct method followed by Fourier syntheses and refined by a full-matrix least-squares method using the SHELX-97 programs.[27] All non-hydrogen atoms in **1**–**5** were refined in an anisotropic approximation, except for the C atoms of one positionally disordered outer ethylene group in the EDT-TTF fragment of the molecule in the structure of **2**. Positions of the H atoms were calculated geometrically with isotropic displacement parameters fixed at 120% (or 150% for the CH_3 and OH groups) of the corresponding parameters of the attached C, O, and N atoms. Torsion angles of idealized hydrogen positions in the CH_3 groups were refined from electron-density coordinates of all of the hydrogen atoms in the structure of **4** only. Details of unit cell data, data collection, and refinement are summarized in Table 4. The structure data for **4** were previously published[16] and are included here for comparison.

CCDC-904667 (for **1**), -904668 (for **2**), -904669 (for **3**), -904670 (for **4**), and -904671 (for **5**) contain the supplementary crystallographic data for this paper. These data can be obtained free of charge from The Cambridge Crystallographic Data Centre via www.ccdc.cam.ac.uk/data_request/cif.

Cyclic Voltammetry: Cyclic voltammetry (CV) experiments were performed in a three-electrode cell equipped with a platinum millielectrode, a platinum wire-counter electrode, and a silver wire used as a quasi-reference electrode. The electrochemical experiments were carried out under a dry and oxygen-free atmosphere (H_2O < 1 ppm, O_2 < 1 ppm). DMF (approximately 0.5 mM) with Bu_4NPF_6 (0.1 M) was used as the supporting electrolyte. Voltammograms were recorded with an EGG PAR 273A potentiostat with positive feedback compensation. On the basis of repetitive measurements, absolute errors on potentials were estimated around ±5 mV. All of the cyclic voltamograms were calibrated versus the oxidation potential of ferrocene.

Supporting Information (see footnote on the first page of this article): ^1H and ^{13}C NMR spectra.

Table 4. Room temperature crystal data, data collection, and refinement details for EDT-TTF-CO-GlyOEt (**1**), EDT-TTF-CO-AlaOEt (**2**), Me_2-TTF-CO-GlyOEt (**3**), EDT-TTF-CO-GlyOH (**4**), and Me_2-TTF-CO-GlyOH (**5**).

	1	**2**	**3**	**4**	**5**
Chemical formula	$C_{13}H_{13}NO_3S_6$	$C_{14}H_{15}NO_3S_6$	$C_{13}H_{15}NO_3S_4$	$C_{11}H_9NO_3S_6$	$C_{11}H_{11}NO_3S_4$
Formula weight	423.60	437.63	361.5	395.55	333.5
Crystal system	monoclinic	monoclinic	triclinic	monoclinic	monoclinic
a [Å]	8.4523(5)	7.7900(4)	7.9942(7)	8.511(1)	10.914(1)
b [Å]	20.543(2)	10.111(2)	10.0510(8)	18.397(2)	8.6629(4)
c [Å]	10.2056(4)	23.441(4)	20.585(2)	10.0007(6)	29.830(3)
α [°]	90	90	90.663(9)	90	90
β [°]	102.742(4)	91.914(7)	90.839(8)	99.635(7)	96.339(9)
γ [°]	90	90	98.158(6)	90	90
V [Å^3]	1728.4(2)	1845.3(4)	1637.0(3)	1543.8(3)	2803.1(4)
Space group, Z	$P2_1/c$, 4	$P2_1$, 4	$P\bar{1}$, 4	$P2_1/c$, 4	$P2_1/n$, 8
$\rho_{calcd.}$ [g/cm^3]	1.628	1.575	1.467	1.702	1.580
μ [cm^{-1}]	8.02	7.54	5.87	8.92	6.79
Θ_{max} [°]	27.02	27.50	29.98	26.49	28.00
Reflections collected	33841	36167	54824	15810	47103
Independent reflections	3754	8167	9381	3163	6730
R_{int}	0.1007	0.0675	0.0609	0.0519	0.0867
Number of variables	209	436	385	217	350
Goodness-of-fit on F^2	1.015	1.003	1.010	1.032	1.001
Final R [$I > 2\sigma(I)$]	0.0356	0.0488	0.0406	0.0473	0.0457

Acknowledgments

The authors thank the RFBR – Centre National de la Recherche Scientifique (CNRS) (grant number 12-03-91059) for the financial support.

[1] M. Bendikov, F. Wudl, D. F. Perepichka, *Chem. Rev.* **2004**, *104*, 4891–4946, and references cited therein.
[2] M. Fourmigué, P. Batail, *Chem. Rev.* **2004**, *104*, 5379–5418.
[3] A. Dolbecq, M. Fourmigué, P. Batail, C. Coulon, *Chem. Mater.* **1994**, *6*, 1413–1418.
[4] A. Dolbecq, A. Guirauden, M. Fourmigué, K. Boubekeur, P. Batail, M.-M. Rohmer, M. Bénard, C. Coulon, M. Sallé, P. Blanchard, *J. Chem. Soc., Dalton Trans.* **1999**, 1241–1248.
[5] P. Blanchard, K. Boubekeur, M. Sallé, G. Duguay, M. Jubault, A. Gorgues, J. D. Martin, E. Canadell, P. Auban-Senzier, D. Jérome, P. Batail, *Adv. Mater.* **1992**, *4*, 579–581.
[6] a) A. S. Batsanov, M. R. Bryce, G. Cooke, J. N. Heaton, J. A. K. Howard, *J. Chem. Soc., Chem. Commun.* **1993**, 1701–1702; b) A. J. Moore, M. R. Bryce, A. S. Batsanov, J. N. Heaton, C. W. Lehmann, J. A. K. Howard, N. Robertson, A. E. Underhill, I. F. Perepichka, *J. Mater. Chem.* **1998**, *8*, 1541–1550.
[7] K. Heuzé, M. Fourmigué, P. Batail, *J. Mater. Chem.* **1999**, *9*, 2373–2379.
[8] S. A. Baudron, N. Avarvari, P. Batail, C. Coulon, R. Clérac, E. Canadell, P. Auban-Senzier, *J. Am. Chem. Soc.* **2003**, *125*, 11583–11590.
[9] O. Neilands, S. Belyakov, V. Tilika, A. Edzina, *J. Chem. Soc., Chem. Commun.* **1995**, 325–326.
[10] Y. Morita, S. Maki, M. Ohmoto, H. Kitagawa, T. Okubo, T. Mitani, K. Nakasuji, *Synth. Met.* **2003**, *135–136*, 541–542.
[11] A. Dolbecq, M. Fourmigué, F. C. Krebs, P. Batail, E. Canadell, R. Clérac, C. Coulon, *Chem. Eur. J.* **1996**, *2*, 1275–1282.
[12] C. Lemouchi, S. Simonov, L. Zorina, C. Gautier, P. Hudhomme, P. Batail, *Org. Biomol. Chem.* **2011**, *9*, 8096–8101.
[13] S. Booth, E. N. K. Wallace, K. Singhak, P. N. Barlett, J. D. Kilburn, *J. Chem. Soc. Perkin Trans. 1* **1998**, 1467–1474.
[14] A. S. Batsanov, S. L. Viles, A. J. Moore, *Acta Crystallogr., Sect. E* **2005**, *61*, o648–o650.
[15] T. Kitamura, S. Nakaso, N. Mizoshita, Y. Tochigi, T. Shimomura, M. Moriyama, K. Ito, T. Kato, *J. Am. Chem. Soc.* **2005**, *127*, 14769–14775.
[16] A. El-Ghayoury, C. Mézière, S. Simonov, L. Zorina, M. Cobian, E. Canadell, C. Rovira, B. Nafradi, B. Sipos, L. Forro, P. Batail, *Chem. Eur. J.* **2010**, *16*, 14051–14059.
[17] a) X. Zhao, S. Zhang, *Chem. Soc. Rev.* **2006**, *35*, 1105–1110; b) J. S. Nowick, *Acc. Chem. Res.* **2008**, *41*, 1319–1330; c) G. Angelici, G. Falini, H.-J. Hofmann, D. Huster, M. Monari, C. A. Tomassini, *Angew. Chem.* **2008**, *120*, 8195; *Angew. Chem. Int. Ed.* **2008**, *47*, 8075–8078.
[18] a) S. A. Baudron, N. Avarvari, P. Batail, C. Coulon, R. Clérac, E. Canadell, P. Auban-Senzier, *J. Am. Chem. Soc.* **2003**, *125*, 11583–11590; b) K. Heuzé, M. Fourmigué, P. Batail, E. Canadell, P. Auban-Senzier, *Chem. Eur. J.* **1999**, *5*, 2971–2976.
[19] M. Fourmigué, E. W. Reinheimer, K. R. Dunbar, P. Auban-Senzier, C. Pasquier, C. Coulon, *Dalton Trans.* **2008**, 4652–4658.
[20] K. Heuzé, M. Fourmigué, P. Batail, *J. Mater. Chem.* **1999**, *9*, 2373–2379.
[21] R. Behrendt, M. Schenk, H.-J. Musiol, L. Moroder, *J. Pept. Sci.* **1999**, *5*, 519–529.
[22] A. S. Batsanov, M. R. Bryce, J. N. Heaton, A. J. Moore, P. J. Skabara, J. A. K. Howard, E. Orti, P. M. Viruela, R. Viruela, *J. Mater. Chem.* **1995**, *5*, 1689–1696.
[23] Y. Lakhdar, C. Mézière, L. Zorina, M. Giffard, P. Batail, E. Canadell, P. Auban-Senzier, C. Pasquier, D. Jérome, B. Nafradi, L. Forro, *J. Mater. Chem.* **2011**, *21*, 1516–1522.
[24] M. Etter, *Acc. Chem. Res.* **1990**, *23*, 120–126.
[25] a) Y. L. Chang, M. A. West, F. W. Fowler, J. W. Lauher, *J. Am. Chem. Soc.* **1993**, *115*, 5991–6000; b) T. Chang, K. Pieterse, M. A. C. Broeren, H. Kooijman, A. L. Spek, P. A. J. Hilbers, E. W. Meijer, *Chem. Eur. J.* **2007**, *13*, 7883–7889.
[26] G. M. Sheldrick, *SADABS*, University of Göttingen, Germany, **1996**.
[27] G. M. Sheldrick, *Acta Crystallogr., Sect. A* **2008**, *64*, 112–122.

Received: October 8, 2012
Published Online: December 19, 2012

